

Poly(2-thiophen-3-yl-malonic acid), a Polythiophene with Two Carboxylic Acids Per Repeating Unit

Oscar Bertran,^{*,‡,†} Elaine Armelin,^{*,‡,§} Francesc Estrany,^{§,||} Alex Gomes,^{‡,⊥} Juan Torras,[#] and Carlos Alemán^{*,‡,§}

Departament de Física Aplicada, EUETII, Universitat Politècnica de Catalunya, Pça Rei 15, Igualada 08700, Spain,
Departament d'Enginyeria Química, ETS d'Enginyers Industrials de Barcelona, Universitat Politècnica de Catalunya, Diagonal 647, Barcelona E-08028, Spain, Center for Research in Nano-Engineering, Universitat Politècnica de Catalunya, Campus Sud, Edifici C', C/Pasqual i Vila s/n, Barcelona E-08028, Spain, Unitat de Química Industrial, EUETIB, Universitat Politècnica de Catalunya, Comte d'Urgell 187, Barcelona 08036, Spain,
Departamento de Tecnología de Polímeros, Faculdade de Engenharia Química, Universidade Estadual de Campinas, Cidade Universitária Zeferino Vaz, Caixa Postal 6066, CEP 13081-970, Campinas-SP, Brazil,
Departament d'Enginyeria Química, EUETII, Universitat Politècnica de Catalunya, Pça Rei 15, Igualada 08700, Spain

Received: January 24, 2010; Revised Manuscript Received: March 10, 2010

A new substituted polythiophene derivative bearing malonic acid, poly(2-thiophen-3-yl-malonic acid), has been prepared and characterized using a strategy that combines both experimental and theoretical methodologies. The chemical structure of this material has been investigated using FTIR and ¹H NMR, and its molecular conformation has been determined using quantum mechanical calculations. Interestingly, the arrangement of the inter-ring dihedral angles was found to depend on the ionization degree of the material, that is, on the pH, which has been found completely soluble in aqueous base solution. Thus, the preferred anti-gauche conformation changes to syn-gauche when the negatively charged carboxylate groups transforms into neutral carboxylic acid. UV-vis experiments and quantum mechanical calculations on model systems with a head-to-tail regiochemistry showed that the lowest $\pi-\pi^*$ transition energy is 2.25 and 2.39 eV for the negatively charged and the neutral polymer, respectively. These values are slightly larger than those previously reported for other polythiophenes with bulky polar side groups. The polymer presents a good thermal stability with a decomposition temperature above 215 °C and an electrical conductivity of 10^{-5} S/cm, which is characteristic of semiconductor materials. Scanning electron microscopy micrographs showed that, after doping, the surface of this material displays regular distribution pores with irregular sizes. This surface suggests that poly(2-thiophen-3-yl-malonic acid) is a candidate for potential applications such as selective membranes for electrodialysis, wastewater treatment, or ion-selective membranes for biomedical uses.

Introduction

Conducting polymers (CPs) are materials with an enormous projection because their optical and electronic properties are useful for a wide number of potential technological applications.^{1–4} Among them, polythiophene derivatives are particularly important, since much progress has been made in the past two decades to solve their serious problems of solubility and processability.^{1,4,5} A widely accepted strategy to overcome such problems consists of the incorporation of substituents into the 3-position of the thiophene ring, which produced not only processable CPs but also allowed the complete chemical and physical characterization

of the prepared materials.^{6–23} Specifically, it was found that the introduction of long alkyl side chains increases the solubility in organic solvents,^{9–12} whereas hydrophilic substituents produce poly(thiophene)s soluble in water or polar solvents.^{13–23}

In recent years, we have particularly focused in the development of poly(thiophene)s with electron-withdrawing carboxylic acid groups in the 3-position of the thiophene ring.^{21–23} Within this field, the work of Heeger and co-workers¹³ on poly(thiophenesulfonate)s was a pioneering contribution to water-soluble CPs influencing subsequent investigations in very similar systems.^{14,15} Electroactive polymers and copolymers with acetic acid, propionic acid, and octanoic acid linked to the thiophene ring have also been investigated.^{16–20} More recently, we reported the synthesis and structural and electronic characterization of poly(3-thiophen-3-yl-acrylic acid methyl ester), poly(3-thiophene-3-yl acrylic acid), and poly(2-thiophen-3-yl-malonic acid dimethyl ester), which are soluble in polar solvents.^{21–23}

In this work, we extend our previous investigations to poly(2-thiophen-3-yl-malonic acid), hereafter abbreviated PT3MA (Scheme 1), a new CP bearing two carboxylate units per thiophene ring. This CP has been derived from the alkaline hydrolysis of the poly(2-thiophen-3-yl-malonic acid dimethyl ester) (PT3MDE in Scheme 1), which was obtained by chemical

* Address correspondence to either author. E-mails: (O.B.) oscar@euetii.upc.es, (E.A.) elaine.armelin@upc.edu, (C.A.) carlos.aleman@upc.edu.

[†] Departament de Física Aplicada, EUETII, Universitat Politècnica de Catalunya.

[‡] Departament d'Enginyeria Química, ETS d'Enginyers Industrials de Barcelona, Universitat Politècnica de Catalunya.

[§] Center for Research in Nano-Engineering, Universitat Politècnica de Catalunya.

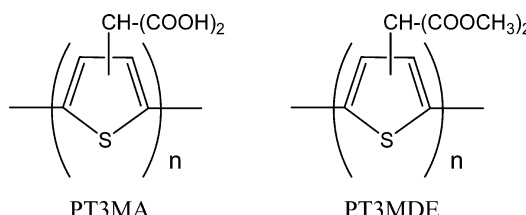
^{||} Unitat de Química Industrial, EUETIB, Universitat Politècnica de Catalunya.

[⊥] Universidade Estadual de Campinas.

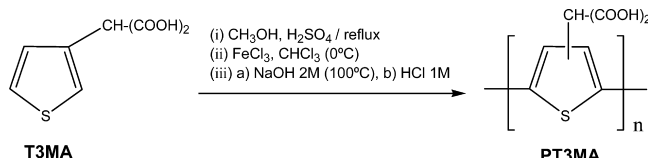
[#] Departament d'Enginyeria Química, EUETII, Universitat Politècnica de Catalunya.

[¶] Both authors contributed equally to this work.

SCHEME 1



SCHEME 2



oxidative coupling polymerization,²³ and subsequently studied using both experimental and theoretical methods.

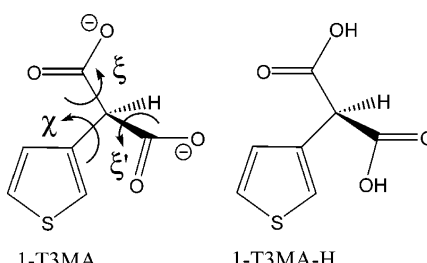
It should be noted that the properties of PT3MA have been investigated using both experimental and theoretical methods that have been used complementarily. Thus, current theoretical methods, and especially the quantum mechanical (QM) ones, are able to describe very satisfactorily the structural and electronic properties of polyconjugated molecules, and nowadays, they should be considered as additional characterization tools. Specifically, for PT3MA, we have characterized the chemical structure by FTIR and NMR, the molecular conformation by QM calculations, the thermal properties by thermogravimetric analyses (TGA), the electronic properties by both UV-vis spectroscopy and QM calculations, and the morphology by scanning electron microscopic (SEM). In addition, the solubility and electrical conductivity of this material have been determined. The resulting properties have been compared with those reported for other polythiophenes bearing substituents with polar groups.

Methods

Experimental Methods. Synthesis. PT3MA was prepared by oxidative coupling polymerization (Scheme 2). For this purpose, the 2-thiophen-3-yl-malonic acid monomer (T3MA) was initially transformed into 2-thiophen-3-yl-malonic acid dimethyl ester (T3MDE) by refluxing (3 g) in dry methanol (15 mL) with 1–2 drops of concentrated sulphuric acid for 24 h (yield: 90%). It should be noted that protection of T3MA is essential to prevent this monomer from oxidative acid decomposition during the polymerization process. More details about this procedure were given in our previous work.²³ The transformation of PT3MDE into PT3MA was performed by alkaline hydrolysis (Scheme 2). For this purpose, the former polymer (~1 g) was stirred in 100 mL of 2 M NaOH solution for 24 h at 100 °C. The resulting mixture was filtered to remove the insoluble part and was poured into 1 M HCl aqueous solution to precipitate PT3MA. This material was repeatedly washed with deionized water and dried under vacuum for 3 days (yield: 82–85%).

Equipment. FTIR spectra were recorded on a 4100 Jasco spectrophotometer equipped with an ATR MKII Golden Gate Heated Single Reflection Diamond Specac accessory. Proton NMR spectra of the monomers (T3MA and T3MDE) and polymers (PT3MA and PT3MDE) were recorded on a Varian Inova 300 spectrometer operating at 300.1 MHz. For this purpose, they were dissolved in deuterated chloroform (CDCl_3) or dimethyl sulfoxide (DMSO). Chemical shifts were calibrated

SCHEME 3



using tetramethylsilane as the internal standard. The thermal stability was examined by TGA using a Perkin-Elmer TGA-6 thermobalance at a heating rate of $20\text{ }^{\circ}\text{C}\cdot\text{min}^{-1}$ under a nitrogen atmosphere. UV-vis optical spectra of PT3MA were obtained from its 1 mg/mL solution in aqueous base using a Shimadzu UV-240 Graphcord UV-vis recording spectrophotometer. SEM photographs of the polymers surface were carried out with a JEOL JSM-6400 scanning electron microscope equipped with an EDS Oxford analyzer.

Theoretical Methods. Molecular Models. Molecular geometries of model oligomers containing n chemical repeating units with n ranging from 1 to 6 were fully optimized using the Hartree–Fock (HF) methodology. Because PT3MA is completely soluble in aqueous base solution (see the Results section), calculations were performed considering both the ionized form (n -T3MA), which presents two negative charges per repeating unit, and the deionized (n -T3MA-H) form of each oligomer (Scheme 3). The HF method was combined with the 6-31+G(d,p) and 6-31G(d,p) basis sets^{24,25} for calculations on n -T3MA and n -T3MA-H, respectively, the extradiffuse function in the treatment of n -T3MA being necessary to improve the description of the electron density. The unrestricted HF formalism (UHF) was considered for negatively charged oligomers; for deionized systems, the restricted formalism was used. The abbreviation used to denote the theoretical level applied to n -T3MA and n -T3MA-H oligomers is UHF/6-31+G(d,p) and HF/6-31G(d,p), respectively. Previous studies indicated that these QM methods provide a very satisfactory description of both the molecular geometry and the energy of heterocyclic oligomers, such as those studied in this work.^{26,27}

Starting geometries for the calculated oligomers were generated considering that two consecutive rings may adopt an anti-gauche ($\theta \approx \pm 145^\circ$) or a syn-gauche ($\theta \approx \pm 40^\circ$) arrangement, where θ refers to the inter-ring dihedral angle defined by the S—C—C—S sequence. Thus, the anti-gauche and syn-gauche dispositions correspond to the global and local energy minima, respectively, typically found in disubstituted 2,2'-bithiophene derivatives, their energy difference being intimately related to both the position and the size of the substituents.^{28,29}

Electronic Properties. The first ionization potentials (IPs) were estimated using the Koopmans' theorem.³⁰ Accordingly, IPs were taken as the negative of the highest occupied molecular orbital (HOMO) energy; that is, $IP = -\epsilon_{HOMO}$. The IP indicates if a given acceptor (p-type dopant) is capable of ionizing, at least partially, the molecules of the compound. The $\pi-\pi^*$ lowest transition energy (ϵ_g) was approximated as the difference between the HOMO and lowest unoccupied molecular orbital (LUMO) energies; that is, $\epsilon_g = \epsilon_{LUMO} - \epsilon_{HOMO}$. Although the HF method provides a satisfactory qualitative description of the electronic properties of polyheterocyclic molecules, we are aware that this theoretical procedure tends to overestimate the values of the IP and ϵ_g .^{31,32} Accordingly, the electronic properties presented in this work have been estimated performing single

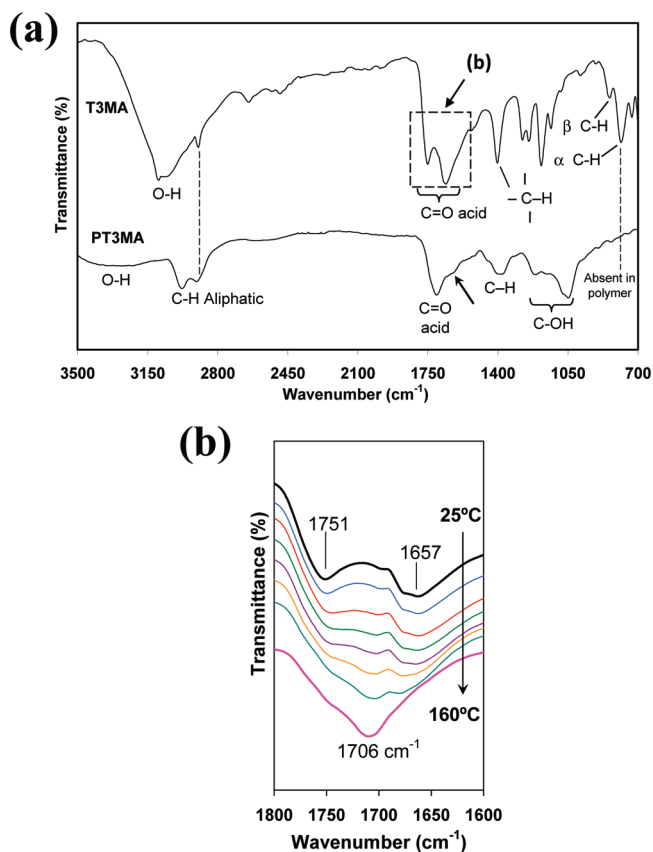


Figure 1. (a) FTIR-ATR spectra of the monomer (T3MA) and polymer (PT3MA). (b) Detail of the carbonyl absorption bands of T3MA in the solid and melted states (from 25 to 160 °C).

point density functional theory (DFT) calculations with the (U)B3PW91^{33,34} method, combined with the 6-31+G(d,p) and 6-31G(d,p) basis sets,^{24,25} on the molecular geometries optimized at the UHF/6-31+G(d,p) and HF/6-31G(d,p) levels, respectively. Electronic properties predicted by this methodological combination and experimental values are expected to be quantitatively comparable. Thus, previous studies on π -polyconjugated systems indicated that the B3PW91 functional is able to reproduce very satisfactorily a wide number of electronic properties.^{21–23,27,35,36} According to the Janak's theorem,³⁷ the approximation mentioned above for the calculation of the IP can be applied to DFT calculations, whereas Levy and Nagy evidenced that ε_g can be rightly approximated as the difference between ε_{LUMO} and ε_{HOMO} in DFT calculations.³⁸

All the QM calculations presented in this work were performed using the Gaussian 03 computer program.³⁹

Results and Discussion

Structural Characterization of PT3MA. Figure 1a compares the FTIR spectra of T3MA and PT3MA. The main absorption bands are listed in Table 1, a comparison with other related CPs such as poly(3-thiophene acetic acid) (P3TAA)¹⁶ and poly(3-hexylthiophene) (PHT)⁴⁰ being also included. Both the success of the chemical oxidative reaction with FeCl₃ and the structure of PT3MDE were previously detailed,²³ and therefore, we concentrate our discussion in the hydrolysis process and the identification of the main absorption bands of PT3MA. The presence of the acid group in both T3MA and PT3MA is clearly detected by the carbonyl absorption region. Two bands, which correspond to the free C=O stretching (1751 cm⁻¹) and C=O associated with intermolecular hydrogen bonds

(1657 cm⁻¹), are clearly separated in the monomer. Furthermore, the O–H stretching vibration associated with intermolecular hydrogen bond is detected as a strong and very broad band at 3400–2700 cm⁻¹. In contrast and as expected, the C=O absorption band, related to the intermolecular hydrogen bond of the carbonyl, is not detected in the polymer, and the C=O stretching vibration changes to 1705 cm⁻¹. Figure 1b, which shows the evolution of the carbonyl absorption bands in T3MA when the temperature increases from 25 to 160 °C, indicates that the absorption band at ~1706 cm⁻¹ corresponds to intramolecular interactions of carbonyl groups forming another hydrogen bond arrangement in the liquid state. Accordingly, the C=O acid group is expected to form intramolecular hydrogen bonds in the PT3MA chain. This assumption is supported by the O–H stretching vibration in PT3MA, which changes to a broad and relatively weak absorption band at 3400–3200 cm⁻¹; that is, this band is characteristic of polymers with hydrogen bonding interactions. Unfortunately, the temperature-dependent FTIR study of the polymer did not provide any additional evidence because of the broadness of the C=O absorption bands (Figure 1a). The C=O stretching vibration of the ester in T3MDE and PT3MDE were detected at 1712 and 1740 cm⁻¹, respectively, and the C–O stretching and the CH₃ asymmetric bending were identified at around 1200 and 1438 cm⁻¹, respectively (Table 1 and reference²³).

The aromatic C–H out-of-plane deformation, which appeared at 785 cm⁻¹ in the monomer, is absent in PT3MA, proving that the polymerization occurs at the α – α' position of the thiophene rings. Although the bands are significantly broader in the polymer than in the monomer, a shoulder (pointed out with an arrow in Figure 1a) can be seen at 1625 cm⁻¹ in the spectrum of PT3MA. This band should be attributed to the C=C bonds of the conjugated structure, which is influenced by the electron-withdrawing group [–CH(COOH)₂].

The molecular structures of T3MA and P3TMA were determined by ¹H NMR spectroscopy, the results being in agreement with their expected chemical structures (Figure 2): T3MA (CDCl₃) δ 12.52 ppm (s, –COOH, 1H), 7.26–7.11 ppm (m, thiophene protons, 3H), 4.86 ppm (s, aliphatic –CH–, 1H); PT3MA (DMSO) δ 12.51 ppm (s, –COOH, 1H), 7.26–7.06 ppm (thiophene protons, 1H), 4.85 ppm (aliphatic –CH–, 1H).

Comparison of the spectra displayed in Figure 2 with those previously reported for T3MDE and PT3MDE allows confirmation of the esterification and hydrolysis steps, since the –COOCH₃ and –OH signals appeared and disappeared as corresponding to each process.²³ Thus, the ester groups of T3MDE were not deteriorated during the oxidative polymerization (peak at 3.7–3.6 ppm on PT3MDE spectrum).²³ As expected, general spectral broadening was observed as a result of the polymerization process. Although the absence of any new peak after the polymerization step suggests the expected α – α' coupling of the thiophene units, the presence of shoulders should be due to the remaining α -H atom at the ring proton multiple region. This is usually associated with relatively low molecular weight polymer molecules. The low molecular weight of the polymer is also evidenced by the peak area of the thiophene proton (peak c in Figure 2), which is larger than that of the aliphatic proton (peak d in Figure 2). In our previous work, we determined the ratio of head-to-tail (HT) and head-to-head (HH) diads arising from polymerization for PT3MDE using the splitting of the –COOCH₃ signal. Specifically, the peak areas of the protons in the 3.7–3.0 ppm region indicated a 75:25 distribution of HT:HH diads, which must be retained in PT3MA.

TABLE 1: Main Infrared Absorption Bands (cm^{-1}) for PT3MA As Well As for the Monomers and Intermediate Compounds^c

compd abreviation (see text)	aromatic C—H in-plane deformation		aliphatic C—H stretch	C=O acid or ester	CH ₃ asymmetric bending	aromatic C—H out-of-plane deformation	
	α	β				α	β
T3MA				1751, 1657		1183, 1244	785
T3MDE			2923, 2853	1740	1438	1261, 1214	798
PT3MDE		3105	2952, 2850	1736	1437	1234, 1153	839
PT3MA			2980, 2900	1705		1212, 1048	
P3TAA ^a		~3000	3000–2800	1700	1410	~ 1200	836
PHT ^b		3055	2959, 2858		1377		825

^a From ref 16. ^b From ref 44. ^c Data reported in the literature for related conducting polymers have been included for comparison.

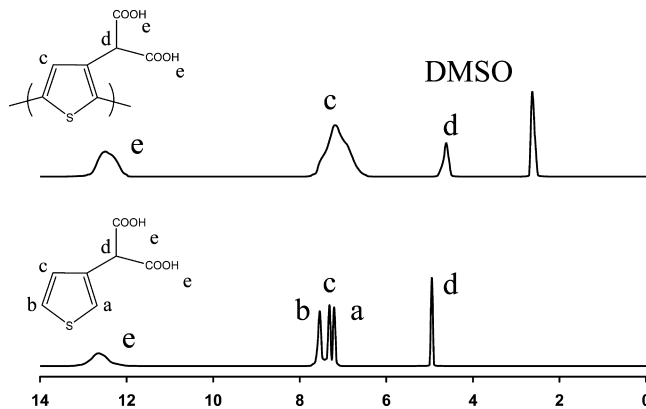


Figure 2. ^1H NMR spectra of T3MA and PT3MA obtained from CDCl_3 and DMSO solutions, respectively.

Conformational Analysis of the Monomer. QM calculations on 1-T3MA and 1-T3MA-H were performed to determine the conformational preferences of the malonic acid side group. The three-dimensional disposition of the substituent in these monomers is defined by the flexible dihedral angles χ , ξ , and ξ' (Scheme 3). Because each of these dihedral angles is expected to exhibit three different minima (i.e., trans (180°), gauche⁺ (60°), and gauche⁻ (-60°)), $3^3 = 27$ theoretical minima can be anticipated for the potential energy hypersurface, $E = E(\chi, \xi, \xi')$, of each monomer. All these structures were used as starting points of 1-T3MA and 1-T3MA-H for full geometry optimizations at the UHF/6-31+G(d,p) and HF/6-31G(d,p) levels, respectively.

Calculations led to four and six minimum energy conformations for 1-T3MA and 1-T3MA-H, respectively, which were distributed within a relative energy interval of 1.8 and 2.9 kcal/mol. These optimized structures are depicted in Figures 3 and 4, which also display the conformational parameters and relative energy (ΔE). In all cases, the driving force that defines the conformation of the substituent is the minimization of the repulsive interactions between the four oxygen atoms. The tendency of the T3MA monomer to form complexes stabilized by intermolecular hydrogen bonds, as it is found by FTIR (Figure 1), was examined in a previous study.⁴¹ Since the energy differences were relatively small, all the minimum energy conformations of both 1-T3MA and 1-T3MA-H were considered in the modeling of the corresponding dimers, that is, 2-T3MA and 2-T3MA-H, respectively.

Conformational Analysis of Dimers: A Molecular Model for Polymer Chains. Calculations on 2-T3MA and 2-T3MA-H were carried out to determine the conformational preferences in terms of both the three-dimensional substituent disposition and the inter-ring dihedral angle (θ). For this purpose, three possible isomers, which differ in the position of the substituents,

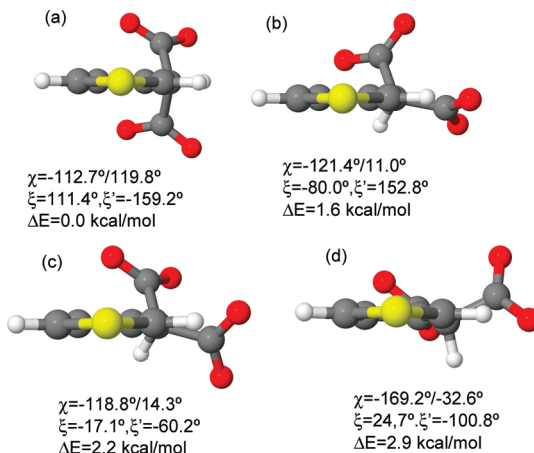


Figure 3. Minimum energy conformations derived for the 1-T3MA monomer from a systematic conformational search. Calculations were performed at the UHF/6-31+G(d,p) level. The dihedral angles of the side group and the relative energy (ΔE) of each minimum are also displayed. Dihedral angles are defined as: $\chi = \text{C}_\alpha(\text{Th})-\text{C}_\beta(\text{Th})-\text{C}-\text{C}(=\text{O})$ (the two complementary values are shown); ξ and $\xi' = \text{C}_\beta(\text{Th})-\text{C}-\text{C}(=\text{O})-\text{O}$ for the branch located above and below the ring, respectively. Th refers to the thiophene ring.

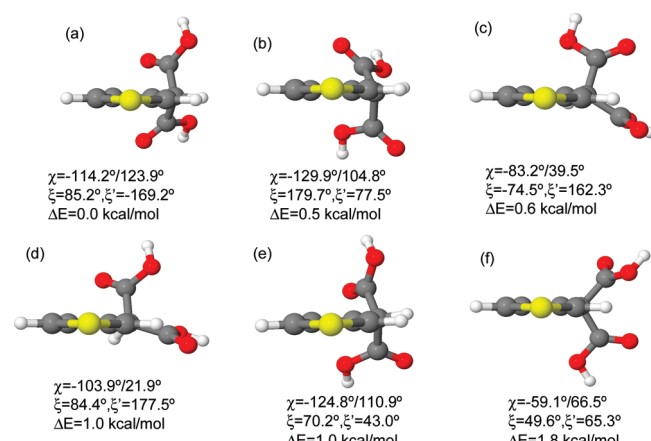


Figure 4. Minimum energy conformations derived for the 1-T3MA-H monomer from a systematic conformational search. Calculations were performed at the HF/6-31G(d,p) level. The dihedral angles of the side group and the relative energy (ΔE) of each minimum are also displayed. Dihedral angles are defined as in Figure 3.

were selected for the negatively charged and the neutral dimers: 4,4' (2-T3MA_{4,4'} and 2-T3MA-H_{4,4'}), 3,3' (2-T3MA_{3,3'} and 2-T3MA-H_{3,3'}), and 3,4' (2-T3MA_{3,4'} and 2-T3MA-H_{3,4'}), which represent the tail-to-tail (TT), head-to-head (HH), and head-to-tail (HT) polymer linkages, respectively. It should be noted that the regiochemistry of polymer chains depends on the attractive or repulsive interactions between monomeric units directly

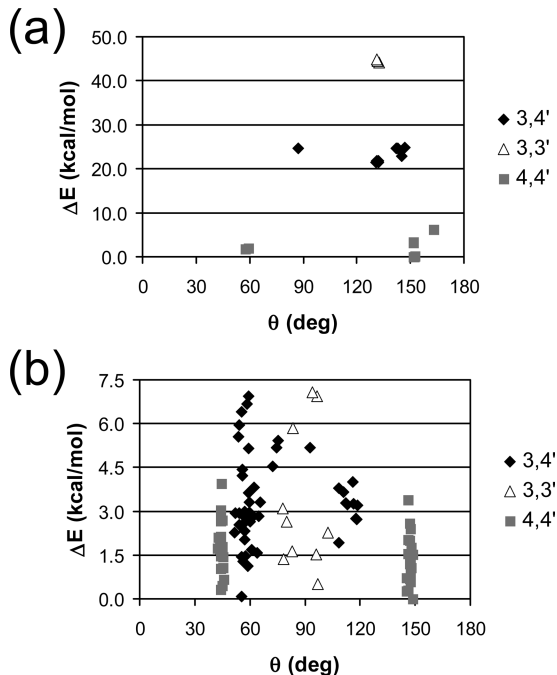


Figure 5. Relative energy (ΔE), calculated with respect to the lowest-energy arrangement of the most stable isomer, against the inter-ring dihedral angle (θ) of all the minima energy conformations found for (a) 2-T3MA_{4,4'}, 2-T3MA_{3,3'}, and 2-T3MA_{3,4'} and (b) 2-T3MA-H_{4,4'}, 2-T3MA-H_{3,3'}, and 2-T3MA-H_{3,4'}.

bonded. Accordingly, regiochemistry can be predicted using simple model molecules formed by two monomeric units rather than large polymer chains.

Results obtained for 1-T3MA and 1-T3MA-H showed that each substituent in the corresponding dimer can adopt 4 and 6 different arrangements (Figures 3 and 4), respectively, which are expected to influence not only the inter-ring dihedral angle but also the relative stability of the different isomers. Consideration of all these arrangements led to construction of 2 minima for the internal rotation of θ , anti-gauche and syn-gauche] \times

$\left\{ \left[m^2 - \binom{m}{2} \right] \right\}$ arrangements of the two side chains, where $m = 4$ and 6 for negatively charged and neutral systems, respectively} = 20 and 42 starting geometries for the 2-T3MA_{4,4'} and 2-T3MA-H_{4,4'}, respectively. The same number was obtained for 2-T3MA_{3,3'} and 2-T3MA-H_{3,3'} isomers, whereas the number of starting structures increased to $2 \times 4^2 = 32$ and $2 \times 6^2 = 72$ for the 2-T3MA_{3,4'} and 2-T3MA-H_{3,4'}, respectively, since the substitutions at positions 3, 4' and 4, 3' are not identical. Accordingly, a total of 72 and 156 starting geometries were considered for 2-T3MA and 2-T3MA-H, respectively.

Complete geometry optimizations led to 8, 3, and 7 minimum energy conformations for 2-T3MA_{4,4'}, 2-T3MA_{3,3'}, and 2-T3MA_{3,4'}, respectively; that is, 18 minima from an initial set of 72 structures, and the number of minima found for 2-T3MA-H_{4,4'}, 2-T3MA-H_{3,3'}, and 2-T3MA-H_{3,4'} was 41, 10, and 47, respectively; that is, 98 minima from an initial set of 156 structures. The distributions of the inter-ring dihedral angle θ against the relative energy for the isomers of two dimers are shown in Figure 5. For each dimer, these distributions have been calculated with respect to the lowest-energy minimum of the most stable isomer. Figures 6 and 7 depict the lowest-energy conformation of each isomer for 2-T3MA and 3-T3MA-H, respectively.

Figure 5a shows that the energies of the 2-T3MA dimer are affected by the electrostatic repulsion between side groups, the

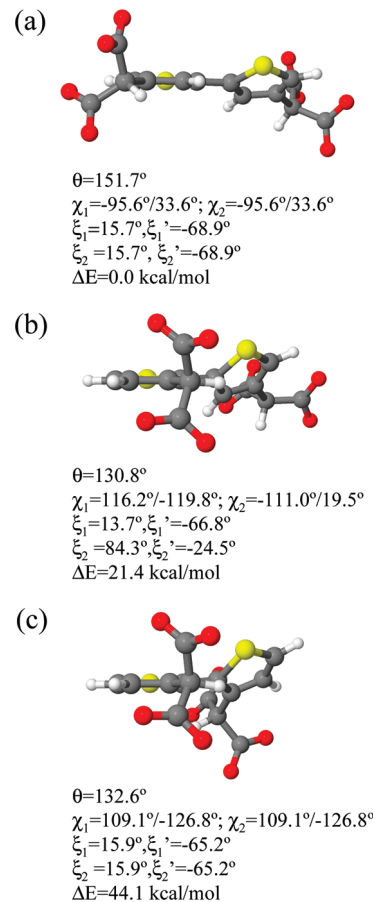


Figure 6. Conformation of lowest energy obtained for (a) 2-T3MA_{4,4'}, (b) 2-T3MA_{3,4'}, and (c) 2-T3MA_{3,3'}. The inter-ring and side chain dihedral angles are listed for each minimum. The dihedral angles have been defined as follows: $\theta = S-C-C-S$; $\chi_i = C_\alpha(\text{Th})-C_\beta(\text{Th})-C-C(=O)$ (the two complementary values are displayed); ξ_i and $\xi_i' = C_\beta(\text{Th})-C-C(=O)-O$ for the branch located above and below the ring, respectively. Th refers to the thiophene ring; $i = 1$ or 2 indicates to the first or second Th in the dimer, respectively.

minimum energy conformations of the three isomers being distributed in groups that are separated by around 20 kcal/mol. The lowest energy conformation corresponds to the 2-T3MA_{4,4'} isomer (Figure 6a), which, as expected, shows the lowest electrostatic repulsion. The inter-ring dihedral angle corresponds to a conventional anti-gauche arrangement in 6 of the 8 minima identified for the 4,4' isomer, whereas the other two are syn-gauche conformations destabilized by 1.8 and 1.9 kcal/mol. Regarding 2-T3MA_{3,4'}, all the minima show an anti-gauche conformation with the exception of one that is arranged perpendicularly, that is, gauche-gauche. These minima are unfavored by about 21–25 kcal/mol with respect to the most stable minimum of 2-T3MA_{4,4'}. Finally, the three minima obtained for 2-T3MA_{3,3'} adopt an anti-gauche arrangement with energies ranging from 44.1 to 44.8 kcal/mol.

On the other hand, 21 of the 98 minima identified for the three 2-T3MA-H isomers are within a relative energy interval of 1.5 kcal/mol (Figure 5b), the inter-ring dihedral angle being arranged in syn-gauche (θ ranges from 44.1° to 45.8°) and anti-gauche (θ ranges from 145.4° to 148.5°) in 7 and 14 of them, respectively. Interestingly, the main difference between the two minima of lowest energy found for 2-T3MA-H_{4,4'} (Figure 7a and b), which differ by only 0.3 kcal/mol, corresponds to the dihedral angle θ , the conformations adopted by the side groups being in both cases very similar to that displayed by

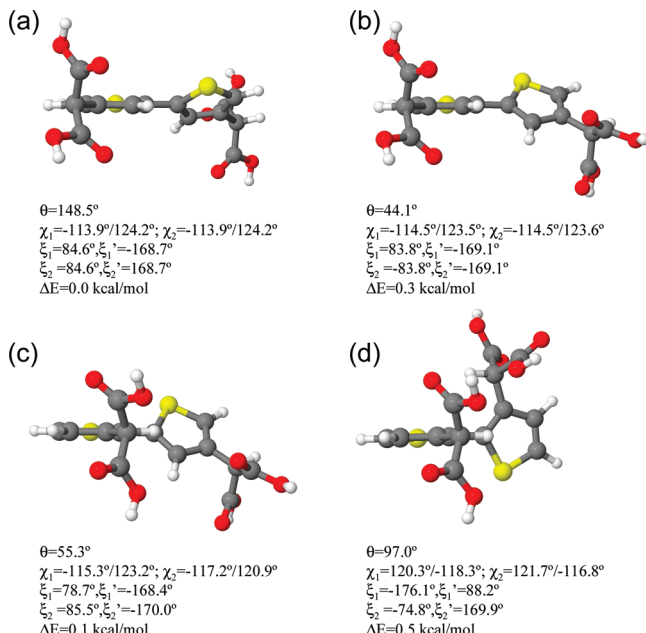


Figure 7. Selected conformations of 2-T3MA-H: (a) lowest energy minimum and (b) first local minimum of 2-T3MA-H_{3,4'} and lowest energy minimum of (c) 2-T3MA-H_{3,4} and (d) 2-T3MA-H_{3,3'}. The inter-ring and side chain dihedral angles are listed for each minimum. Dihedral angles have been defined as in Figure 6.

1-T3MA-H monomer (Figure 4a). Moreover, the lowest energy conformation of 2-T3MA-H_{3,4'} (Figure 7c), which corresponds to a syn-gauche arrangement and is destabilized by only 0.1 kcal/mol, also shows the same conformation for the substituents.

Results displayed in Figure 5b reveal that no minimum with a conventional anti-gauche conformation, that is, $\theta \approx 150^\circ$, was detected for 2-T3MA-H_{3,4'}. This should be attributed to the repulsive interaction between the substituent attached to the C₃-position and the sulfur atom of the neighboring ring, which induces a distortion of $\sim 30\text{--}40^\circ$ in the inter-ring dihedral angle, that is, θ ranges from 108.2° to 118.6° . Furthermore, 2-T3MA-H_{3,4'} presents five minima within a relative energy interval of 1.5 kcal/mol with a syn-gauche conformation; that is, θ ranges from 55.3° to 58.8° . Finally, 2-T3MA-H_{3,3'} is destabilized by 0.5 kcal/mol (Figure 7d) because of the steric interactions induced by the substituents. All the minima identified for this isomer adopt a gauche-gauche conformation, three of them being within a relative energy interval 1.5 kcal/mol.

The rotational energy profiles of 2-T3MA_{3,4'} and 2-T3MA-H_{3,4'} were calculated by scanning the inter-ring dihedral angle θ in steps of 15° between 0° and 360° and considering that the side groups were arranged as in the respective lowest-energy minimum (Figures 6b and 7c, respectively). Calculations were performed considering a flexible rotor approximation: each point of the path was obtained from geometry optimization of the molecule at a fixed value of θ . The resulting potential energy curves, which are displayed in Figure 8, provide more insights about the significant stability of the syn-gauche conformation predicted for the 3, 4' isomers.

The potential energy curve calculated for 2-T3MA_{3,4'} shows two minima at $\theta = 131.2^\circ$ and -138.0° , which are almost isoenergetic. In these conformations, which are separated by the syn ($\theta = 0^\circ$) and anti ($\theta = 180^\circ$) barriers (11.4 and 1.97 kcal/mol, respectively), the inter-ring dihedral angle deviates $\sim 10\text{--}20^\circ$ with respect to the conventional anti-gauche arrangement because of the strong repulsions between the carboxylate groups of the adjacent rings. Moreover, such electrostatic

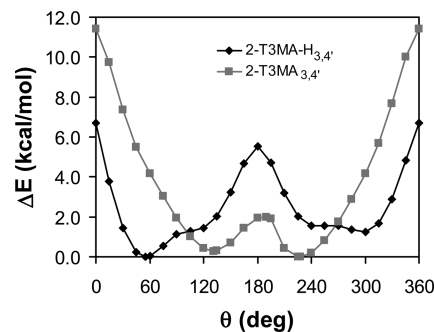


Figure 8. Potential energy curves obtained for the internal rotation of 2-T3MA_{3,4'} and 2-T3MA-H_{3,4} as a function of the inter-ring dihedral angle θ . Calculations were performed at the UHF/6-31+G(d,p) and HF/6-31G(d,p) levels, respectively. Energies are relative to the lowest-energy minimum of each dimer.

TABLE 2: Relative Energy (ΔE ; in kcal/mol) and Inter-Ring Dihedral Angles (θ_1 and θ_2 ; in degrees) Obtained for 3-T3MA-H (see text) at the HF/6-31G(d,p) Level

	A	B	C
ΔE	3.1	1.6	0.0
θ_1	115.5	55.3	53.8
θ_2	116.6	115.6	54.3

repulsions are also responsible for the annihilation of the syn-gauche conformations as local energy minima. In contrast, for the 2-T3MA-H_{3,4'}, the only minimum energy conformations were the syn-gauche⁺ ($\theta = 55.3^\circ$) and syn-gauche⁻ ($\theta = -60.1^\circ$), the latter being unfavored by 1.2 kcal/mol with respect to the former. Thus, the annihilation of the anti-gauche minima should be attributed to the steric interactions between the substituent and the sulfur atom of the adjacent ring. The syn-gauche minima are separated by two barriers located at the syn ($\theta = 0^\circ$) and anti ($\theta \approx 180^\circ$) arrangements of 6.7 and 5.5 kcal/mol, respectively.

To ascertain if the stability of the syn-gauche arrangements found for the neutral system is retained when the polymer chain grows, three trimers, 3-T3MA-H, were constructed. In all three, the positions of the substituents, which were arranged as in the most stable conformation of 2-T3MA_{3,4'} (Figure 7c), were 3, 4', 3''. Initially, the inter-ring dihedral angles θ_1/θ_2 were anti-gauche⁺/anti-gauche⁺ (A), anti-gauche⁺/syn-gauche⁺ (B) and syn-gauche⁺/syn-gauche⁺ (C). Table 2 lists the relative energy and the inter-ring dihedral angles after geometry optimization at the HF/6-31G(d,p) level. As can be seen, θ_1 and θ_2 remained close to the initial values in the three cases, and in addition, the substituents also retained the initial arrangements (data not shown). Furthermore, C was the most stable structure, A and B being unfavored by 3.1 and 1.6 kcal/mol.

It should be noted that polymerization of 2-T3MA_{4,4'} units, which is the most stable isomer of the charged dimer, produces an alternation of head-to-head and tail-to-tail linkages. The large energy penalty associated with the tail-to-tail linkages, that is, the 2-T3MA_{3,3'} isomer, is destabilized by more than 44 kcal/mol with respect to the 2-T3MA_{4,4'} (Figure 5a), which allows one to discard this structural model for PT3MA. In contrast, polymerization of the 3, 4' isomer provides a repetitive sequence of head-to-tail linkages, which is expected to be more stable. This feature was corroborated in previous theoretical studies involving other substituted poly(thiophene)s.^{21,22} The same physical principles can be applied to the 2-T3MA-H isomers, even though the energy differences among the different isomers of the neutral dimer are significantly smaller than those found

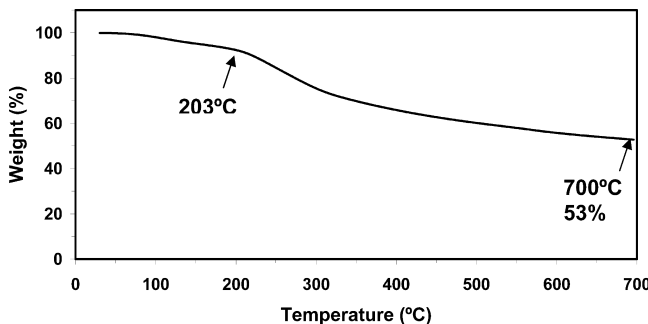


Figure 9. TGA curve (recorded at 20 °C/min of heating rate and from 30 to 700 °C) of PT3MA.

for 2-T3MA. A molecular model in which head-to-tail polymer linkages are repeated along the chain is consistent not only with the ¹H NMR data reported in this work but also with the molecular model previously predicted for PT3MDE.²³

Solubility and Thermal Properties. PT3MA is completely insoluble not only in common organic solvents, such as chloroform, dichloromethane, acetone, and toluene, but also in neutral water. However, it dissolves completely in aqueous base solutions, pH 10–12; almost entirely in dimethyl sulfoxide; and partially in both tetrahydrofuran and dichloroacetic acid. Furthermore, PT3MA also becomes partially soluble in ethanol when the temperature is increased. We note that the solubility properties changed with time (becoming more insoluble), which should be attributed to aggregation phenomena induced by the rearrangement of the polymer chains. The solubility of PT3MA is worse than that of PT3MDE, the latter being completely soluble in acetone, dichloromethane, chloroform, tetrahydrofuran, dimethyl sulfoxide, dichloroacetic acid, and toluene.²³ These results are consistent with our previous results on poly(3-thiophene-3-yl acrylic acid),²² which was much less soluble than the corresponding ester derivatives.²¹

TGA was performed, scanning from 30 to 700 at 20 °C/min. In Figure 9, PT3MA shows an onset of weight loss at around 100°, which should be attributed to the loss of the water molecules trapped in the polymeric matrix. After such a water loss, PT3MA presents only one decomposition process at 250 °C, which has been attributed to the polymer degradation. This represents a significant difference with respect to PT3MDE, which showed a two-step decomposition process.²³ In addition, the remaining weight percentage at 700 °C is considerably higher for PT3MA than for PT3MDE (53% and 18%, respectively), indicating that the content of inorganic residues in the former is significant.

Electronic Properties. Model molecules for negatively charged and neutral PT3MA were built using *n*-T3MA and *n*-T3MA-H oligomers, respectively, with head-to-tail polymer linkages and with *n* ranging from 2 to 6. More specifically, for ionized PT3MA one model (**i-I**) with all the inter-ring dihedral angles initially arranged in the anti-gauche conformation was constructed, whereas two models that differ in the syn-gauche (**d-I**) and anti (**d-II**) conformation of the inter-ring dihedral angles were considered for deionized PT3MA. The following calculations were performed for the *n*-oligomers of each model. Complete geometry optimizations were carried out for **d-I**; partial geometry optimizations were carried out for **d-II**; and finally, **i-I** was subjected to both complete and partial geometry optimizations. In all cases, partial geometry optimizations were performed by fixing the inter-ring dihedral angles at 180°. Previous studies suggested that, to extrapolate the electronic properties calculated for oligomers to infinite chain polymers,

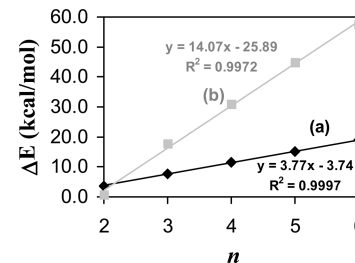


Figure 10. Variation of the energy difference between (a) models **d-I** (syn-gauche conformation) and **d-II** (fixed anti conformation) against *n* for *n*-T3MA-H oligomers; (b) models **i-I** after complete (anti-gauche conformation) and partial (fixed anti conformation) geometry optimization against *n* for *n*-T3MA oligomers.

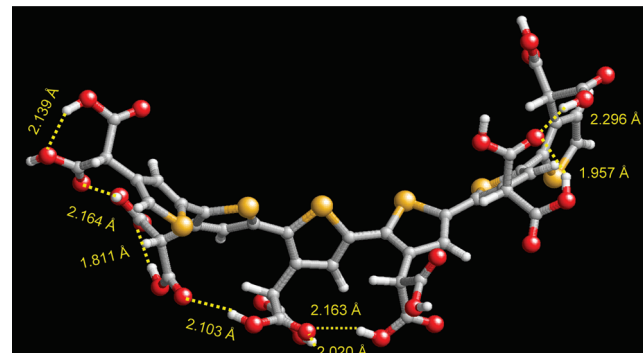


Figure 11. Molecular model with intramolecular hydrogen bonds proposed for neutral PT3MA.

conformational defects should be avoided by imposing an all-anti conformation.⁴² However, the latter conformation is strongly destabilized in the case of *n*-T3MA-H oligomers with head-to-tail linkages due to the large size of the substituent. Figure 10 shows the variation of the energy difference between the structures of *n*-T3MA-H derived from geometry optimization of **d-I** and **d-II** against *n*. The stability of the former model increases with the molecular size; that is, 3.1 kcal/mol per repeating unit. Figure 10 also includes the energy difference between the structures obtained for **i-I** after complete and partial geometry optimizations against *n*. As can be seen, an energy penalty of ~9.6 kcal/mol per repeating unit is produced in the negatively charged system when the inter-ring dihedral angles are fixed at 180°.

The side chains of model **d-I** can be easily rearranged to form a network of intramolecular hydrogen bonds. It should be noted that the formation of these interactions is not possible when the molecular model of the polymer is generated by repeating systematically the lowest energy conformation obtained for the 2-T3MA-H_{3,4'} dimer. Thus, these interactions, which involve not only the carboxylic acid groups of neighboring repeating units but also of the same repeating unit, are possible only when the conformation of the side groups located at adjacent dimers is different. The formation of intramolecular hydrogen bonds, which are illustrated in Figure 11 for 6-T3MA-H, is fully consistent with the FTIR spectrum displayed in Figure 1 for PT3MA. Furthermore, comparison of the model **d-I** with and without an intramolecular hydrogen bond indicates that the former is favored by about 3–4 kcal/mol per repeating unit, that is, the exact value depends on the number of hydrogen bonding interactions as well as their intra- or inter-residue nature.

Figure 12 shows the UV spectrum recorded for PT3MA in aqueous base solution. The first absorption band on the low energy side of the spectra arises from the $\pi-\pi^*$ transition in the delocalized electron system along the chain. Thus, the energy

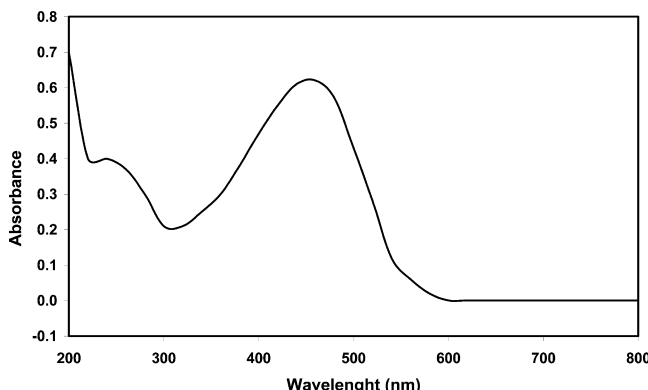


Figure 12. UV-vis spectrum of PT3MA in aqueous base solution.

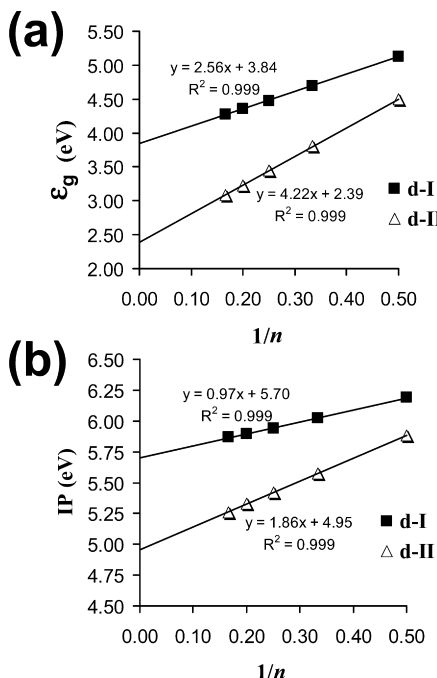


Figure 13. Variation of (a) ϵ_g (in eV) and (b) IP (in eV) against $1/n$, where n is the number of repeat units, for n -T3MA-H oligomers. Models **d-I** (triangles) and **d-II** (squares) with the inter-ring dihedral angles arranged in syn-gauche and anti conformations, respectively, have been considered. The gray lines correspond to the linear regressions used to extrapolate these electronic properties toward infinite polymer systems.

of the band gap of the conduction can be estimated from the intersection of the tangent placed over the inflection point of this curve and the wavelength axes. The ϵ_g value estimated from the UV-vis spectrum in aqueous base is 2.25 eV. This value is considerably lower than that recently obtained for PT3MDE in acetone (2.75 eV).²³ This should be attributed to the effect of the counterions associated with carboxylate groups, which are probably increases in the doping level of PT3MA.

To evaluate the ϵ_g and IP of PT3MA, single point calculations at B3PW91/6-31G(d,p) were performed on the optimized geometries of the n -T3MA-H oligomers, respectively. Unfortunately, UB3PW91/6-31+G(d,p) single point calculations on the UHF/6-31+G(d,p) geometries of n -T3MA oligomers did not converge due to the large number of negative charges. Accordingly, the ϵ_g and IP of PT3MA have been calculated considering the neutral oligomers only. Figure 13 shows the linear variation of ϵ_g and IP against $1/n$ obtained for the **d-I** and **d-II** models of P3TMA. Linear regression analyses, which are included in Figure 13, allowed extrapolation of ϵ_g /IP values

of 3.84/5.70 and 2.39/4.95 eV for an infinite chain of PT3MA, which adopts an all-syn-gauche (**d-I**) and an all-anti (**d-II**) conformation, respectively. The dependence of these two electronic properties on the polymer conformation is very strong. Thus, the variation of the relative arrangement between consecutive thiophene rings from ideal anti to the syn-gauche and, consequently, the loss of planarity, increases the ϵ_g and the IP by 1.45 and 0.75 eV, respectively.

Comparison of the ϵ_g predicted for the PT3MA chain with that calculated for related CPs using a similar theoretical level and an idealized all-anti conformation (e.g., poly(3-thiophene-3-yl acrylic acid methyl ester), 2.28 eV;²¹ poly(3-thiophene-3-yl acrylic acid), 2.12 eV;²² and polythiophene (PT), 1.82 eV³⁵) indicates that the bulky side group is responsible not only for the drastic geometrical distortions showed above but also for the significant increase in the lowest transition energy, which should be related to a diminution of the optical properties. The ϵ_g and IP values calculated for ionized n -T3MA did not show linear behavior compared to $1/n$ (data not shown), which should be attributed to the large number of negative charges in each of such oligomers. Thus, the omission of counterions seems to be a handicap for the prediction of the electronic properties of PT3MA.

The HOMA index⁴³ has been calculated for all the n -T3MA and n -T3MA-H oligomers. This parameter, which provides information about the aromatic character, is based on the C–C and C–S bond length alternation pattern along the π -system:

$$\text{HOMA} = 1 - \frac{\alpha}{l} \sum_{i=1}^l (R_{\text{opt}} - R_i)^2 \quad (1)$$

where l is the number of bonds, α is an empirical constant ($\alpha = 257.7$ and 94.09 for C–C and C–S bonds, respectively), R_i is the bond length, and R_{opt} is the optimal bond length ($R_{\text{opt}} = 1.388$ and 1.677 Å for C–C and C–S bonds, respectively). The HOMA is equal to zero for a Kekulé structure formed by a typical aromatic system with single and double bonds arranged alternatively and is equal to 1 for a system with all bonds equal to the optimal value ($R_i = R_{\text{opt}}$).

Figure 14 shows the evolution of the HOMA index and the averaged inter-ring distance against the number of repeating units, n , determined for model **i-I** of n -T3MA (after both complete and partial geometry optimizations) and models **d-I** and **d-II** of n -T3MA-H. The HOMA index presents linear behavior, even although there is a significant difference between negatively charged and neutral oligomers (Figure 14a). For n -T3MA-H oligomers, the HOMA index increases when n displays a positive convergence, whereas a negative slope is obtained for the n -T3MA systems. Thus, the aromatic character of n -T3MA decreases when n increases, the same feature being also reflected by the positive slope of the average inter-ring distance (Figure 14b). In contrast, the averaged inter-ring distance remains constant at $1.470 \text{ \AA} \pm 0.001 \text{ \AA}$ for both **d-I** and **d-II** when n increases from 2 to 6 (data not shown). The behavior of the ionized system must be attributed to the Coulombic repulsion between adjacent repeating units, which acts against the electronic charge delocalization. A similar behavior was previously detected for poly(thiaheterohelicene) CPs.⁴⁴

Morphology and Electrical Conductivity. Because no morphological investigation was reported in our previous study on poly(3-thiophene-3-yl acrylic acid), a polythiophene derivative with the carboxylic acid group separated from the polymer

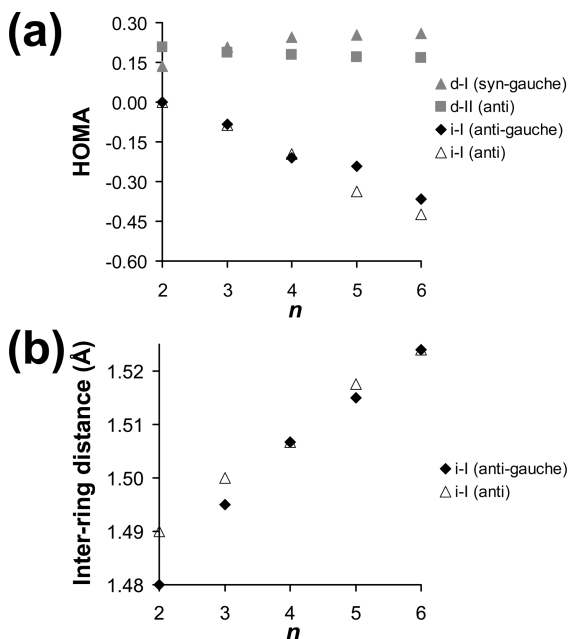
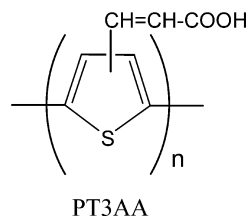


Figure 14. Variation of (a) the aromaticity index HOMA against the number of monomer units (n) for model **i-I** of n -T3MA after complete and partial geometry optimizations (inter-ring dihedral angles in anti-gauche and anti, respectively) and for models **d-I** and **d-II** of n -T3MA-H (inter-ring dihedral angles in syn-gauche and anti, respectively); and (b) the inter-ring distance (in Å) against the number of monomer units (n) for model **i-I** of n -T3MA after complete and partial geometry optimizations.

SCHEME 4



backbone by a double bond (PT3AA in Scheme 4), in this section we study the surface of both PT3MA and PT3AA before and after doping with FeCl_3 . Representative SEM micrographs of these four systems are provided in Figure 15).

PT3MA displays a small globular surface as compared with the densely packed irregular surface morphology of PT3AA. Interestingly, the surface of the two polymers becomes significantly different after doping. More specifically, cellular structures with uniformly distributed pores and irregularly shaped pores were found for doped PT3AA and doped PT3MA, respectively. It is well-known that polymer chains are significantly affected by the doping process, which enhances the planarity of the molecules. Thus, the cauliflower-like structures observed in electron micrographs of typical heterocyclic CPs (polypyrrole, polythiophene, etc.) was attributed to the planarity of the chains.^{3,4} However, here we present CPs with porous structure in the doped state. In addition, in the case of doped PT3AA, the distribution and size of the pores was very regular (Figure 15d), the average diameter being $4 \mu\text{m}$. It should be noted that the doping-induced porosity cannot be attributed to the vacuum-drying process because of the homogeneous and narrow size distribution obtained. Results displayed in Figure 15 suggest that some CPs bearing carboxylic acid substituents relatively close to the π -system, such as PT3MA and especially PT3AA, are very promising material for selected and specific

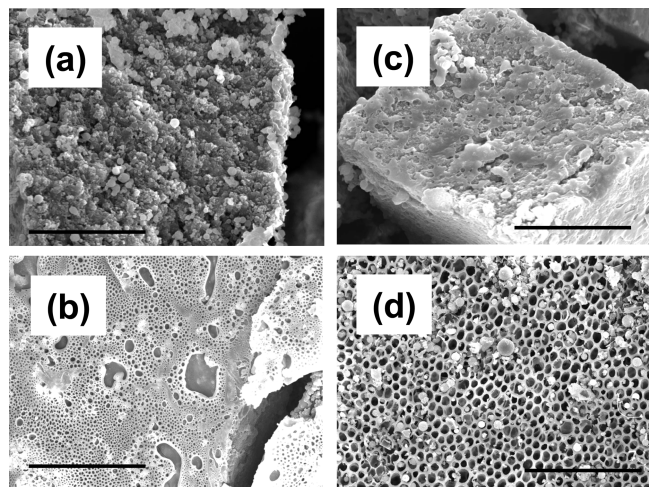


Figure 15. SEM micrographs of (a) PT3MA before doping; (b) PT3MA doped with 25% of FeCl_3 ; (c) PT3AA before doping; and (d) PT3AA doped with 25% FeCl_3 ; Scale bar: 40 μm (a, c), 80 μm (b, d).

applications; for example, membranes for separation, matrixes for the immobilization of enzymes, and drug delivery systems. Doping-induced volume changes were previously reported for other polythiophene derivatives.⁴⁰

The electrical conductivity was determined after doping with FeCl_3 using the standard four-probe technique. Measurements were performed on pellets of the doped polymer, which were prepared by applying a pressure of 6 tons. The resulting conductivities were very low, $\sim 10^{-5} \text{ S/cm}$, which is in agreement with results previously obtained for PT3AA.²² Unfortunately, it was not possible to prepare samples of PT3MA using a modification of the layer-by-layer polymerization-doping technique,⁴⁵ because it was previously used to produce PT3MDE samples on glass plates.²³ Thus, the resulting PT3MA films were very porous, and in addition, it was difficult to remove from the glass plates. The difficulties found in the preparation of the PT3MA samples, which resulted in a poor alignment of the polymer chains, should be attributed to the large content of inorganic ions (dopant ions and counterions for the carboxylate groups). It should be noted that the electrical conductivity determined for PT3DME applying the four-probe technique on these samples was 6 S/cm ,²³ which is significantly higher than that of the carboxylic acid derivative.

Conclusions

PT3MA has been prepared by oxidative coupling polymerization. This material, which is completely soluble in aqueous base solution and partially soluble in a number of polar solvents, has been characterized using a complementary combination of experimental and theoretical techniques. Specifically, we have determined the chemical structure (FTIR and NMR spectroscopy), the molecular conformation (quantum mechanical calculations), the electronic (UV-vis spectroscopy and quantum mechanical calculations) and thermal (TGA) properties, the morphology (SEM), and the electrical conductivity (four probe technique). We concluded that the most stable conformation, which is obtained by repeating head-to-tail linkages, depends on the pH. Thus, calculations on n -T3MA indicate that inter-ring dihedral angles prefer an anti-gauche arrangement, whereas the preferred conformation is the syn-gauche when the carboxylic acid side groups are protonated. This represents a significant difference with respect to typical substituted polythiophenes, in which the anti-gauche conformation is always

preferred. The lowest $\pi-\pi^*$ transition energy found for PT3MA is slightly larger than typically found for other polythiophenes with bulky polar side groups. This must be attributed to the repulsion between adjacent repeating units, which is detrimental to the charge delocalization and the aromatic character. Analyses of the morphology at the PT3MA and PT3AA surfaces show that the compact structures of these materials transform into cellular structures with a uniform distribution of pores upon doping with FeCl_3 . It is particularly remarkable that in the case of doped PT3AA, the pores show a regular shape and size. These porous structures are significantly different from that typically found in doped heterocyclic CPs, suggesting a number of potential applications; for example, selective membranes and drug-delivery systems.

Acknowledgment. This work has been supported by MI-CINN and FEDER funds (Project No. MAT2009-09138) and by the DIUE of the Generalitat de Catalunya (Contract Nos. 2009SGR925 and XRCQTC). A.G. acknowledges financial support from the Euro Brasilian Windows agency (Grant No. 41309-EM-1-2008-PT-ERAMUNDUS-ECW-L16) for his 6-month stay at the UPC. The authors are indebted to the Centre de Supercomputació de Catalunya (CESCA) for the computational resources provided. Support for the research of C.A. was received through the prize ICREA Academia for excellence in research funded by the Generalitat de Catalunya.

References and Notes

- (1) Mishra, A.; Ma, C. Q.; Baüerle, P. *Chem. Rev.* **2009**, *109*, 1141.
- (2) Roncali, J. *Chem. Rev.* **1997**, *97*, 173.
- (3) Skotheim, T. A.; Reynolds, J. R. In *Handbook of Conducting Polymers*, 3rd ed.; CRC Press: Boca Raton, 2007.
- (4) Chan, H. S. O.; Ng, S. C. *Prog. Polym. Sci.* **1998**, *23*, 1167.
- (5) Barbarella, G.; Melucci, M.; Sotgiu, G. *Adv. Mater.* **2005**, *17*, 1581.
- (6) Sato, M.; Tanaka, S.; Kaeriyama, K. *J. Chem. Soc. Chem. Commun.* **1986**, *873*.
- (7) Jen, K. Y.; Miller, G. G.; Elsenbaumer, R. L. *J. Chem. Soc. Chem. Commun.* **1986**, *1346*.
- (8) Bryce, M. R.; Chissel, A.; Kathirgamanathan, P.; Parker, D.; Smith, N. R. M. *J. Chem. Soc. Chem. Commun.* **1987**, *6*, 466.
- (9) Chen, T. A.; Wu, X.; Rieke, R. D. *J. Am. Chem. Soc.* **1995**, *117*, 233.
- (10) Hsu, W.-P.; Levon, K.; Ho, K.-S.; Myerson, A. S.; Kwei, T. K. *Macromolecules* **1993**, *26*, 1318.
- (11) Yang, C.; Orfino, F. P.; Holdcroft, S. *Macromolecules* **1996**, *29*, 6510.
- (12) McCullough, R. D. *Adv. Mater.* **1998**, *10*, 93.
- (13) Patil, O. A.; Ikenoue, Y.; Wudl, F.; Heeger, A. J. *J. Am. Chem. Soc.* **1987**, *109*, 1858.
- (14) Chayer, M.; Faïd, K.; Leclerc, M. *Chem. Mater.* **1997**, *9*, 2902.
- (15) Masuda, H.; Kaeriyama, K. *Makromol. Chem., Rapid Commun.* **1992**, *13*, 461.
- (16) Kim, B.; Chen, L.; Gong, J.; Osada, Y. *Macromolecules* **1999**, *32*, 3964.
- (17) Liaw, D. J.; Liaw, B. Y.; Gong, J. P.; Osada, Y. *Synth. Met.* **1999**, *99*, 53.
- (18) Welzel, H. P.; Kossmehl, G.; Stein, H. J.; Schneider, J.; Plieth, W. *Electrochim. Acta* **1995**, *40*, 577.
- (19) Visy, C.; Kankare, J.; Kriván, E. *Electrochim. Acta* **2000**, *45*, 3851.
- (20) Ewbank, P. C.; Loewe, R. S.; Zhai, L.; Reddinger, J.; Sauvé, G.; McCullough, R. D. *Tetrahedron* **2004**, *60*, 11269.
- (21) Bertran, O.; Pfeiffer, P.; Torras, J.; Armelin, E.; Estrany, F.; Alemán, C. *Polymer* **2007**, *48*, 6955.
- (22) Bertran, O.; Armelin, E.; Torras, J.; Estrany, F.; Codina, M.; Alemán, C. *Polymer* **2008**, *49*, 1972.
- (23) Armelin, E.; Bertran, O.; Estrany, F.; Salvatella, R.; Alemán, C. *Eur. Polym. J.* **2009**, *45*, 2211.
- (24) Frisch, M. J.; Pople, J. A.; Binkley, J. S. *J. Chem. Phys.* **1984**, *80*, 3265.
- (25) Hariharan, P. C.; Pople, J. A. *Chem. Phys. Lett.* **1972**, *16*, 217.
- (26) Alemán, C.; Domingo, V.; Fajará, Ll.; Julià, L.; Karpfen, A. *J. Org. Chem.* **1998**, *63*, 1041.
- (27) Alemán, C.; Casanova, J. *J. Phys. Chem. A* **2004**, *108*, 1440.
- (28) Ocampo, C.; Curcò, D.; Alemán, C.; Casanova, J. *Synth. Met.* **2006**, *156*, 602.
- (29) Alemán, C.; Julià, L. *J. Phys. Chem.* **1996**, *100*, 1524.
- (30) Koopmans, T. *Physica* **1934**, *1*, 104.
- (31) Gatti, C.; Frigerio, G.; Benincori, T.; Brenna, E.; Sannicolò, F.; Zotti, G.; Zecchin, S.; Schiavon, G. *Chem. Mater.* **2000**, *12*, 1490.
- (32) Alemán, C.; Armelin, E.; Iribarren, J. I.; Liesa, F.; Laso, M.; Casanova, J. *Synth. Met.* **2005**, *149*, 151.
- (33) Becke, A. D. *J. Chem. Phys.* **1993**, *98*, 1372.
- (34) Perdew, J. P.; Wang, Y. *Phys. Rev. B* **1992**, *45*, 13244.
- (35) Casanova, J.; Zanuy, D.; Alemán, C. *Polymer* **2005**, *46*, 9452.
- (36) Casanova, J.; Alemán, C. *J. Phys. Chem. C* **2007**, *111*, 4823.
- (37) Janak, J. F. *Phys. Rev. B* **1978**, *18*, 7165.
- (38) Levy, M.; Nagy, A. *Phys. Rev. A* **1999**, *59*, 1687.
- (39) Frisch, M. J.; Trucks, G. W.; Schlegel, H. B.; Scuseria, G. E.; Robb, M. A.; Cheeseman, J. R.; Montgomery, J. A.; Vreven, T., Jr.; Kudin, K. N.; Burant, J. C.; Millam, J. M.; Iyengar, S. S.; Tomasi, J.; Barone, V.; Mennucci, B.; Cossi, M.; Scalmani, G.; Rega, N.; Petersson, G. A.; Nakatsuji, H.; Hada, M.; Ehara, M.; Toyota, K.; Fukuda, R.; Hasegawa, J.; Ishida, M.; Nakajima, T.; Honda, Y.; Kitao, O.; Nakai, H.; Klene, M.; Li, X.; Knox, J. E.; Hratchian, H. P.; Cross, J. B.; Adamo, C.; Jaramillo, J.; Gomperts, R.; Stratmann, R. E.; Yazyev, O.; Austin, A. J.; Cammi, R.; Pomelli, C.; Ochterski, J. W.; Ayala, P. Y.; Morokuma, K.; Voth, G. A.; Salvador, P.; Dannenberg, J. J.; Zakrzewski, V. G.; Dapprich, S.; Daniels, A. D.; Strain, C. M.; Farkas, O.; Malick, D. K.; Rabuck, A. D.; Raghavachari, K.; Foresman, J. B.; Ortiz, J. V.; Cui, Q.; Baboul, A. G.; Clifford, S.; Cioslowski, J.; Stefanov, B. B.; Liu, G.; Liashenko, A.; Piskorz, P.; Komaromi, I.; Martin, R. L.; Fox, D. J.; Keith, T.; Al-Laham, M. A.; Peng, C. Y.; Nanayakkara, A.; Challacombe, M.; Gill, P. M. W.; Johnson, B.; Chen, W.; Wong, M. W.; Gonzalez, C.; Pople, J. A. *Gaussian 03, Revision B.02*; Gaussian, Inc.: Pittsburgh, PA, 2003.
- (40) Yoshino, K.; Nakao, K.; Onoda, M.; Sugimoto, R. *Solid State Commun.* **1989**, *70*, 609.
- (41) Casanova, J.; Bertran, O.; Armelin, E.; Torras, J.; Estrany, F.; Alemán, C. *J. Phys. Chem. A* **2008**, *112*, 10650.
- (42) Ocampo, C.; Casanova, J.; Liesa, F.; Alemán, C. *Polymer* **2006**, *47*, 3257.
- (43) Krygowski, T. M. *J. Chem. Inf. Comput. Sci.* **1993**, *33*, 70.
- (44) Torras, J.; Bertran, O.; Alemán, C. *J. Phys. Chem. B* **2009**, *113*, 15196.
- (45) Nicolau, Y. F.; Daried, S.; Genoud, F.; Nechtschein, M.; Travers, J. P. *Synth. Met.* **1991**, *42*, 1491.